International Journal of Solids and Structures 48 (2011) 3112–3127

Contents lists available at ScienceDirect

International Journal of Solids and Structures

journal homepage: www.elsevier.com/locate/ijsolstr

A new constitutive model for shear banding instability in metallic glass

H.H. Ruan [a,*], L.C. Zhang [a], J. Lu [b]

[a] School of Mechanical & Manufacturing Engineering, The University of New South Wales, Sydney, NSW 2052, Australia
[b] College of Science and Engineering, City University of Hong Kong, Hong Kong, China

ARTICLE INFO

Article history:
Received 4 October 2010
Received in revised form 1 July 2011
Available online 20 July 2011

Keywords:
Metallic glass
Constitutive relation
Shear band
Instability
Bifurcation
Flow serration

ABSTRACT

Inelastic deformation of metallic glass is through shear banding, characterized by significantly localized deformation and emerged expeditiously under certain stress state. This study establishes a new constitutive model addressing the physical origin of the shear banding. In the modeling, the atomic structural change and the free volume generation are embodied by the plastic shear strain and the associated dilatation. The rugged free energy landscape is adopted to naturally reflect the rate-independent flow stress and flow serrations. Based on this, the conditions for the onset of shear banding instability are established, which enables the explicit calculation of the shear band inclination angle and its extension speed. The study concludes that shear band angle is significantly influenced by the diltancy factor and pressure sensitivity, that a shear band does not increase its thickness once emanated from a deformation unit, that the spreading speed of a shear band is intersonic, and that more shear bands, which lead to higher ductility, can be induced by high strain rates or by the introduction of a second material phase. The analysis also demonstrates that the ductility of metallic glass depends on the sample geometry and/or the stress state.

1. Introduction

When metallic glass is loaded, either quasi-statically or dynamically, the formation of shear bands and the localized deformation are the most striking phenomenon which has never been observed in crystalline counterparts. It was therefore believed that the shear bands manifest the major distinction between metallic glass and crystalline metals in terms of atomic structures and their response to external loading. In crystalline metals, lattice defects can easily be nucleated and transmitted, resulting in a low yield stress. In contrast, the plastic deformation of metallic glass has to be the cooperative rearrangements of clusters of atoms, leading to a much higher yield stress. Furthermore, in crystalline metals the lattice defects can be effectively pinned by obstacles like grain boundaries, stacking faults and solute atoms, which brings about strain-hardening and large ductility. In metallic glass, however, once the rearrangement of atoms is activated at a critical stress level, it spreads across the material and traps the deformation, and hence causes the material's brittleness. The plasticity and strain-hardening of crystalline metals have been successfully explained by dislocation dynamics. However, the fundamental understanding of the nucleation, propagation and annihilation of shear bands in metallic glass is still lacking. Questions like how fast a shear band extends or at what conditions a shear band nucleates or annihilates have not yet been convincingly answered.

While the experimental evidence on the physical origin of shear band remains inconclusive, the deformation mechanisms of metallic glass have been investigated theoretically, such as Steif et al. (1982), Huang et al. (2002) and Jiang and Dai (2009). Based on the free volume theory (Spaepen, 1977), they ascribed the inhomogeneous deformation to the shear-induced dilatation which leads to the reduction of viscosity. The adiabatic thermal softening was the secondary effect in the analysis by Jiang and Dai (2009). By assuming a preexisting band with slightly higher initial free volume concentration, Huang et al. (2002), Jiang and Dai (2009) and Gao et al. (2007) studied the instability in the material. They ascribed the instability to the precipitous drop of viscosity within the shear band as the shear stress reached a critical value. Their model has been prevailing in finite-element simulations (Su and Anand, 2006a; Thamburaja and Ekambaram, 2007; Yang et al., 2006), aiming to more precisely simulate the large deformation of metallic glass at high temperature or to investigate the shear band activation and fracture at low temperature (Tandaiya et al., 2009).

In the aforementioned modeling of metallic glass, the material was assumed to be viscoelastic. The free volume concentration, which varies with the stress state, serves as an internal variable to correlate the microstructure defect with the macroscopic deformation rate. This assumption is useful in establishing high-temperature stress–strain relationships, in which the stress

* Corresponding author.
E-mail address: haihui.ruan@gmail.com (H.H. Ruan).

0020-7683/$ - see front matter © 2011 Elsevier Ltd. All rights reserved.
doi:10.1016/j.ijsolstr.2011.07.004

overshoot and the non-Newtonian behavior can be well described (Thamburaja and Ekambaram, 2007). However, the direct extension of this theory to a low-temperature scenario has faced significant challenges.

The first challenge is that the viscoelasticity within the theory makes the flow stress at low temperature significantly rate-sensitive (Jiang and Dai, 2009), while experimental evidence clearly shows that the yield stress of metallic glass is insensitive to strain rate (Schuh et al., 2007). To resolve this problem, Anand and Su (2005) simply assumed that the yield surface is weakly dependent on or independent of the strain rate. However, this assumption breaks the connection between the microstructure defects and the macroscopic deformation rate.

In addition to the rate-dependency, the previous models cannot describe the serrations (or pops) at experimental stress–strain curves, which was ascribed to the shear band nucleation and annihilation (Song et al., 2008; Wang et al., 2009a). Both the viscoelastic model and the elastoplastic model render smooth stress-strain curves and merely a single load drop after the formation of catastrophic shear bands. Therefore, it is necessary to develop a new model to describe the physical origin of these serrations.

The third challenge is the shear band propagation. To our knowledge, no method for calculating the speed of shear band is available. The estimation of shear-banding speed from experimentally measured data varies from a few meters per second (Wright et al., 2009) to the speed of a shear wave (Lewandowski and Greer, 2006), supported by the dynamic strain measurement (Wright et al., 2009), high-speed photography (Sunny et al., 2009) and molecular dynamic simulations (Cao et al., 2009).

The present study will take up the above challenges by developing a new theoretical model that not only considers viscous deformation rate in BMG but also the associated atomic structural change of the material. The free energy undulating with the peaks and basins will be treated as the evolution of the material's atomic structure.

2. Constitutive modeling

2.1. Thermodynamics requirement

Consider the variation of free energy Φ of the atomic subsystems in metallic glass over the atomic coordinates as a hypersurface in a high-dimensional space. If the change of atomic coordinates due to the far-field shear stress τ is in a corporative manner and can be described by one or several proportional parameters, say the shear strain γ, a path of deformation can be identified on the hypersurface. This path has peaks and valleys, corresponding to many activated states and basin states. The second law of thermodynamics requires non-negative dissipation rate (Maugin, 1992), which reads

$$(\tau - \partial\Phi/\partial\gamma)\dot{\gamma} \geqslant 0. \tag{2.1}$$

Integrating Eq. (2.1) yields

$$Q \equiv \text{dissipation} = \int_{\gamma_1}^{\gamma_2} \tau d\gamma - (\Phi|_{\gamma=\gamma_1} - \Phi|_{\gamma=\gamma_2}), \tag{2.2}$$

where $\gamma = \gamma_1$ and $\gamma = \gamma_2$ represent two different atomic structures in the adjacent basins along the deformation path. Particularly, if $\Phi|_{\gamma=\gamma_1} = \Phi|_{\gamma=\gamma_2}$, the external work $\int_{\gamma_1}^{\gamma_2} \tau d\gamma$ associated with this transition is totally dissipated. $\gamma_0 = \gamma_2 - \gamma_1$ is regarded as the plastic strain since it refers to the irreversible change of atomic structures. It is worth highlighting that the jump from one energy basin to another is a dynamic process once the energy barrier is overcome. In experimental observations, γ_0 is embodied by the strain burst in a stress-mediated process. This intermittence, which has also been revealed in crystalline materials (Dimiduk et al., 2006), may be considered as the fundamental feature of plastic deformation.

In order to satisfy Eq. (2.1), we follow Eyring's concept (Eyring, 1936) to express the strain rate as:

$$\dot{\gamma} = \dot{\gamma}_0 \sinh((\tau - \partial\Phi/\partial\gamma)/\tau_0), \tag{2.3}$$

where $\dot{\gamma}_0$ is a reference strain rate and τ_0 is a reference stress. τ_0 may be further expressed as $\tau_0 = K_B T/\Omega_0$, where K_B and T are Boltzmann constant and temperature, respectively, and Ω_0 is the activation volume. Eq. (2.3) renders the strain rate effect of the system. It is noted that if τ_0 is sufficiently small (say less than 5% of the quasi-static yield stress of the material), the yield stress is then dictated by the local maximum of $\partial\Phi/\partial\gamma$. Any significant deviation from the equilibrium (*i.e.*, $\tau = \partial\Phi/\partial\gamma$) should invoke fast atomic motion to re-establish the equilibrium. Noting that the free energy landscape is rate-independent, the local maximum of $\partial\Phi/\partial\gamma$ is also rate-independent. We conjecture that this is the main cause of rate-independency of the yield stress when deforming metallic glass at low rate and low temperature. This conjecture is consistent with the accounts proposed by Johnson and Samwer (2005) and by Schuh et al. (2007). According to Pan et al. (2008), the activation volume Ω_0 of zirconium-based metallic glass is approximately $0.1 \sim 0.3\text{nm}^3$ corresponding to the volume of the shear transformation zone $2.5 \sim 6.6\ \text{nm}^3$. Therefore, at room temperature τ_0 is 10–40 MPa, which is indeed much smaller than the shear strength of metallic glass.

Eq. (2.3) leads to negligible but still positive rate sensitivity. Although from some dynamic experiments, negative strain-rate sensitivity was concluded (Li et al., 2003; Trexler and Thadhani, 2010), we think that it may be induced by artifacts (*e.g.*, stress concentrations) in dynamic experiments as pointed out by Sunny et al. (2007). Li et al. (2003) ascribed the negative rate sensitivity to the early development of a shear band from a local weak region with the yield stress lower than the macroscopic yield stress. In quasi-static case, one is still able to obtain the increase of macroscopic stress due to the relaxation and response of overall material. But for dynamic case, such an early shear band immediately leads to fracture due to the large kinetic energy. In this sense, the negative rate sensitivity refers to the local failure strength rather than the relationship between stress and strain rate. Gu et al. (2003) ascribed the negative rate sensitivity to the adiabatic heating, which in constitutive level is thermal softening rather than negative rate sensitivity at a constant temperature.

If the difference between the driven stress τ and the internal resistance $\partial\Phi/\partial\gamma$ is smaller than τ_0, the system behaves like a Newtonian flow; *i.e.*, $\tau - \partial\Phi/\partial\gamma \approx \tau_0\dot{\gamma}/\dot{\gamma}_0$. For a quasi-static stable process, $\dot{\gamma}$ approaches zero. The measured stress then reflects the internal resistance to the structural change, *i.e.*,

$$\tau = \partial\Phi/\partial\gamma. \tag{2.4}$$

It should be noted that Eq. (2.4) is only applicable before the onset of the shear band, since the deformation within the shear band must be dynamic.

2.2. The kinetics within a shear band

The inelastic deformation of metallic glass is generally embodied by the corporative rearrangement of the atomic subsystems. A two-dimensional schematic of such rearrangement is shown in Fig. 1(a). The figure illustrates an atomic process that accommodates a plastic shear strain γ_0. We try to unify the two distinct views of inelastic deformation of metallic glass, namely, the "shear transformation" after Argon (1979) and the "atomic jump" after Spaepen (1977). According to Argon (1979), the fundamental unit process underlining inelastic deformation is achieved by the shear distortion of a cluster of atoms (in dark grey color) from one relatively low energy configuration (above the arrow) to a second

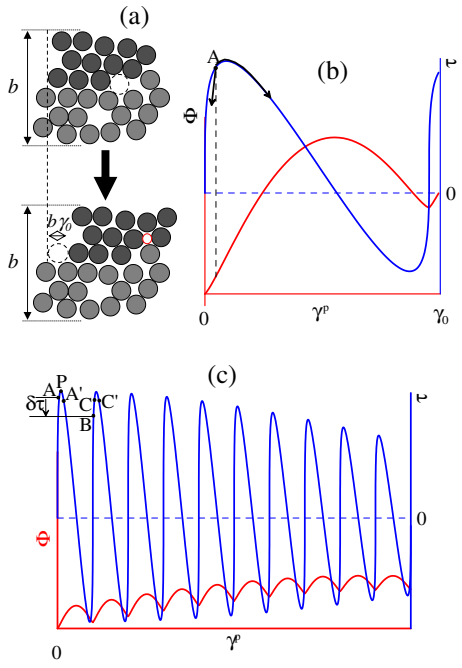

Fig. 1. Shear transformation in metallic glass: (a) a two-dimensional schematic of an atomic subsystem in an amorphous metal; (b) the variation of the free energy and the effective shear stress associated with a deformation unit; (c) the schematic of the free energy landscape and the quasi-periodic change of the effective shear stress.

such configuration (below the arrow). According to Spaepen (1977), this process is the result of a series of atomic jumps into the neighboring free volume (denoted by the dashed circle). As a consequence, the free volume migrates across several atoms to the rightmost position in Fig. 1(a), resulting in a shear offset $b\gamma_0$, where b is the size of the deformation unit.

It is necessary to distinguish the deformation unit in this study from the shear transformation zone (STZ) proposed by Argon (1979). Since we formulate our theory in the framework of continuum mechanics, the deformation unit should represent a sufficiently large cluster of atoms to make the assumption of continuity valid. In Section 3, we will justify that the size of a deformation unit should be the width of the shear band. In contrast, the size of STZ, based on the consideration that the correlation of atomic positions vanishes (Zink et al., 2006), is in the order of 1 nm, which should be regarded as the size of the structural defect. A deformation unit may be considered as an atomic subsystem containing many STZs, which are encompassed by densely packed atoms.

The shear transformation shown in Fig. 1(a) demonstrates the following two fundamental standpoints of the present study:

(1) Due to the amorphous nature of atomic arrangement, both the atomic configurations in Fig. 1(a) are low energy configurations and the transformation crosses an activated state of higher energy;
(2) Associated with the shearing of the subsystem, the volume of the atomic cluster changes. The dilatancy strain is given by $\beta\gamma^p$, where β is the dilatancy factor after Rudnicki and Rice (1975). It should be noted that β is unnecessarily a constant, which can be a function of the stress–strain history. For example, Spaepen's formulation (Spaepen, 1977) can be adapted to account for the free volume generation, which is a result of squeezing an atom into the neighboring hole of a smaller volume. However, in this study, we treat β as a constant.

Now, we take off the elastic response γ^e from the total strain γ. The variation of the free energy Φ with the plastic shear strain γ^p is sketched in Fig. 1(b) (Schuh and Lund, 2003). Differentiating Φ with respect to γ^p renders the internal resistance to plastic deformation. Fig. 1(b) shows that the rise of $\partial\varphi/\partial\gamma^p$ at the infinitesimal γ^p is precipitous. This is in line with the fact that with a small strain, the material is mainly deformed elastically. The negative shear resistance in Fig. 1(b) indicates that as the atomic configuration reaches the unstable transition state, it must transform to the lower energy state even without the application of an external stress. Bifurcation would then be possible as the resolved shear stress reaches the vicinity of the maximum value of $\partial\varphi/\partial\gamma^p$, say Point A in Fig. 1(b). After this point, some zones would be further deformed while other portions would be unloaded. The zones being deformed further can self-organize to the shear bands, of which the dynamic process is the propagation of shear-banding instability.

The deformation within the shear band, through continuous transformation from a low energy state to another, should be resisted quasi-periodically. Here, we use "quasi" to indicate that the period and amplitude may vary with deformation. The Peierls concept (Peierls, 1940; Rice, 1992) is still adaptable here for the cooperative shear transformation, although it was originally proposed for the lattice resistance to dislocation motion in crystalline metals. In metallic glass, this short-range quasi-periodic force is probably the only resistance to inelastic deformation since there are no long-range obstacles. Fig. 1(c) shows schematically the quasi-periodic variations of the free energy and the associated internal resistance. The overall trend of the free energy is upward as strain increases. The maximum potential energy corresponds to maximum distortion and alienation of atoms (Shimizu et al., 2006), implying the occurrence of fracture. In addition, the local undulation of the potential energy, known as the β-relaxations (Stillinger, 1995), renders the short-range undulation of the internal resistance to plastic deformation, of which the amplitude may continuously decrease with plastic strain, reflecting softening of the material.

2.3. Shear induced dilatation

Now, let us seek a way to generalize the above shear stress–shear strain relationship to an arbitrary stress state. First, let us incorporate the dilation effect into the dissipation inequality, which leads to:

$$(\sigma_m - \partial\Phi/\partial\varepsilon_v^p)\dot{\varepsilon}_v^p + (\bar{\tau} - \partial\Phi/\partial\gamma^p)\dot{\gamma}^p \geqslant 0, \tag{2.5}$$

where $\bar{\tau} = \sqrt{\sigma'_{ij}\sigma'_{ij}/2}$ is the equivalent shear stress, σ'_{ij} are the deviatoric stresses, $\sigma_m = \sigma_{ii}/3$ is the hydrostatic stress, and $\dot{\varepsilon}_v^p$ is the plastic dilatancy strain rate. The repeated indices imply summation herein and hereafter. The elastic strains are neglected in the above expression since they are reversible and non-dissipative. Substituting the relationship $\dot{\varepsilon}_v^p = \beta\dot{\gamma}^p$ and rearranging Eq. (2.5), we get the basic expression Eq. (2.1) back, *i.e.*, $(\tau - \partial\Phi/\partial\gamma^p)\dot{\gamma}^p \geqslant 0$, where

$$\tau = \bar{\tau} + \mu\sigma_m \tag{2.6a}$$

and the internal frictional coefficient μ is given by

$$\mu = \beta\left(1 - \frac{\partial\Phi}{\sigma_m\partial\varepsilon_v^p}\right). \tag{2.6b}$$

It is noted that if the free energy is insensitive to the plastic volumetric strain, *i.e.*, $\partial\Phi/\partial\varepsilon_v^p = 0$, the normality rule, $\mu = \beta$, is recovered (Storen and Rice, 1975).

In the above deduction, we have assumed that the plastic volumetric strain, attributed to the free volume generation, is merely correlated to the equivalent plastic shear strain. This assumption

may however be too naive to model the actual behavior of metallic glass. Noting that the equivalent plastic strain is always non-negative, the consequence of this assumption is the non-negative volume change after deformation. This inference would probably be problematic since the free volume may vary due to the significant hydrostatic stresses. In this case, Eq. (2.5) should be used instead of Eq. (2.6a). We shall consider the pressure induced plastic volumetric strain in our successive works. In this paper, we only consider the shear induced dilatation for simplicity.

Eq. (2.6a) demonstrates that the effective shear stress depends on the hydrostatic stress rather than the normal stress at a particular shear plane. This is the distinction between Drucker–Prager model and Mohr–Coulomb model. Zhao and Li (2008) discussed the fundamental problem when adopting Mohr-Coulomb model and they demonstrated that Drucker–Prager model has been adequate to interpret the shear band inclination angle in uniaxially loaded metallic glass. Experimental investigations by Lu et al. (2003) also suggest that a pressure-dependent yielding surface should be more appropriate since the shear band inclination angle was not consistent with the variation of Mohr circles in a biaxial stress state. We believe this is true based on the following reasons:

(i) For uniaxially loaded metallic glass, the difference between tensile and compressive fracture stresses is generally less than 10% (reference is listed in Table 1). The internal frictional coefficient should therefore be less than 0.05. This is generally far from the value calculated from the shear band angle when adopting the Mohr–Coulomb model.
(ii) Metallic glass is isotropic without any preexisting shear plane. The yield surface should be initially smooth without any vertex. However, the yield surface from the Mohr–Coulomb criterion is unsmooth. On the other hand, The smooth version of the Mohr-Coulomb criterion (*e.g.*, Matsuoka–Nakai yield criterion (Matsuoka and Nakai, 1974)) requires three stress invariants and several calibration parameters, which are hard to be quantified and have not been proved necessary for metallic glass.
(iii) The primary reason for adopting the Mohr–Coulomb model is to explain the diversified shear band inclination angles of many types of metallic glasses (Zhang et al., 2003a). However the dilatancy factor β also affects the shear band angle significantly as to be discussed in Section 4.2. Therefore, the Mohr–Coulomb model may not be the best choice.

The experimental results on the biaxial or triaxial yield surface of metallic glass are yet insufficient for deterministic conclusion, while atomistic simulations provide an alternative way to investigate the problem. Schuh and Lund (2003) published their simulation result of the biaxial yield surface of $Cu_{50}Zr_{50}$metallic glass. Their data are replicated in Fig. 2. Although the authors interpreted their results using the Mohr–Coulomb yield criterion, we found that the Drucker–Prager model renders a much more precise description of the data as shown in Fig. 2.

2.4. Triaxial stress–strain relations

The generalization of the above shear with dilatation model to triaxial stress–strain relations follows the standard process in the theory of plasticity. Nevertheless, since metallic glass yields at a much larger strain than a conventional metal, we shall incorporate the effect of large deformation. Refer to the instantaneous configuration of the material points, the instantaneous rates of the deformation and spin tensors are given by

$$\dot{\varepsilon}_{ij} = (\partial v_i/\partial x_j + \partial v_j/\partial x_i)/2, \quad \Omega_{ij} = (\partial v_i/\partial x_j - \partial v_j/\partial x_i)/2, \tag{2.7}$$

respectively, where v_i and x_i denotes the particle velocities and material coordinates respectively. The Jaumann rate of the true stress σ_{ij} is then given by Storen and Rice (1975)

$$\overset{\nabla}{\sigma}_{ij} = \dot{\sigma}_{ij} + \Omega_{ki}\sigma_{kj} + \sigma_{ik}\Omega_{kj}, \tag{2.8}$$

where the overhead dot denotes the time derivative at a fixed material point and the overhead ∇ denotes the Jaumann rate.

Now consider a quasi-static process before the bifurcation point. The approximate condition (2.4) leads to:

$$\overset{\nabla}{\tau} = \frac{d\tau}{d\gamma^p}\dot{\gamma}^p = \frac{\partial^2 \Phi}{\partial(\gamma^p)^2}\dot{\gamma}^p = h\dot{\gamma}^p, \tag{2.9}$$

where $h = \partial^2\Phi(\gamma^p)/\partial\gamma^{p^2}$ is the instantaneous hardening rate. Invoking Φ as the plastic potential and noting that $\partial\Phi/\partial\tau = \tau/h$, we get the deviatoric components of plastic strain rate tensor as

$$\dot{e}^p_{ij} = \dot{\lambda}\frac{\partial\Phi}{\partial\sigma_{ij}} = \dot{\lambda}\frac{\tau}{h}\frac{\sigma'_{ij}}{2\bar{\tau}}, \tag{2.10}$$

where $\dot{e}^p_{ij} = \dot{\varepsilon}^p_{ij} - \frac{1}{3}\dot{\varepsilon}^p_{kk}\delta_{ij}$. Since $\dot{\gamma}^p = \sqrt{2\dot{e}^p_{ij}\dot{e}^p_{ij}}$, we have

$\dot{\lambda} = h\dot{\gamma}^p/\tau$.

Eq. (2.10) is then recast as

$$\dot{e}^p_{ij} = \dot{\gamma}^p\frac{\sigma'_{ij}}{2\bar{\tau}}. \tag{2.11}$$

Substituting Eq. (2.9) into Eq. (2.11) and including the elastic and volumetric response lead to the following Jaumann stress rate–strain rate relation

$$\dot{\varepsilon}_{ij} = \frac{\overset{\nabla}{\sigma'}_{ij}}{2G} + \frac{\overset{\nabla}{\sigma}_{kk}}{9K}\delta_{ij} + \frac{\sigma'_{ij}\overset{\nabla}{\tau}}{2h\bar{\tau}} + \frac{\beta\overset{\nabla}{\tau}}{3h}\delta_{ij}, \tag{2.12}$$

where G and K are shear and bulk moduli, respectively, δ_{ij} is Kronecker tensor, and

$$\overset{\nabla}{\tau} = \overset{\nabla}{\bar{\tau}} + \mu\overset{\nabla}{\sigma}_m = \frac{\sigma'_{kl}}{2\bar{\tau}}\overset{\nabla}{\sigma}_{kl} + \frac{\mu}{3}\overset{\nabla}{\sigma}_{kk}.$$

Table 1
A comparison of compressive and tensile strength of metallic glass.

Material	Tensile strength (GPa)	Tensile fracture angle	Compressive strength (Gu et al.)	Compressive fracture angle (°)	Difference in strength (%)	References
$Zr_{59}Cu_{20}Al_{10}Ni_8Ti_3$	1.6	54°	1.7	43°	6	Zhang et al. (2003a)
$Zr_{48}Cu_{45}Al_7$	1.71 ± 0.08	n/a	1.85 ± 0.05	n/a	8	Wu et al. (2008), Yao et al. (2008)
$Zr_{40}Ti_{12}Ni_{9.4}Cu_{12.2}Be_{26.4}$	1.978 ± 0.02	50°–53°	2.0 ± 0.069	39°–41°	5	Lewandowski and Lowhaphandu (2002)
$Zr_{52.5}Ni_{14.6}Al_{10}Cu_{17.9}Ti_5$	1.66 ± 0.42	55°–65°	1.82 ± 0.13	40°–45°	9	He et al. (2001)
$Cu_{60}Zr_{30}Ti_{10}$	2.15	54°	2.0	n/a	7	Inoue et al. (2001)
$Cu_{60}Hf_{25}Ti_{15}$	2.16	n/a	2.13	n/a	1	Inoue et al. (2001)
$La_{62}Al_{14}(Cu,Ni)_{24}$	0.549	90°	0.561	40°–45°	2	Lee et al. (2004)
$Zr_{52.5}Ni_{14.6}Cu_{17.9}Al_{10}Ti_5$	1650	54°	1850	45° ± 1°	10	Liu et al. (1998)

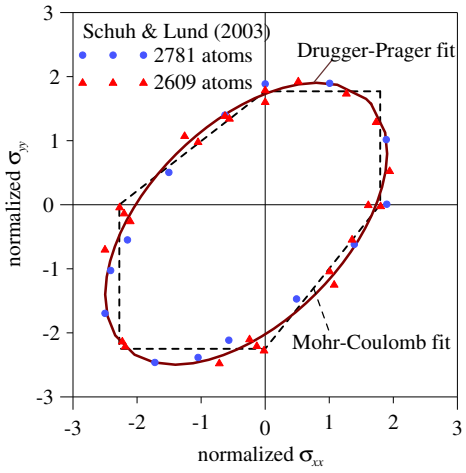

Fig. 2. The biaxial yield surface of $Cu_{50}Zr_{50}$ (Schuh and Lund, 2003).

3. Kinetic conditions of bifurcation

With the constitutive model established above, let us now investigate the general conditions for shear-banding instability. We postulate that the shear band forms at the state where the high-order rate of deformation can bifurcate from the homogenous field and that the shear band forms instantaneously across the sample at the incipient instability. Without losing generality, let us consider a shear band in the x_1–x_2 plane as shown in Fig. 3(a), where the unit normal and tangential vectors $\boldsymbol{n}$ and $\boldsymbol{m}$ shown in Fig. 3(a) are

$$n_1 = \sin\theta, \quad n_2 = \cos\theta, \quad m_1 = -\cos\theta, \quad m_2 = \sin\theta.$$

In the following, the subscripts i, j, k, l, m, n take the value of 1 or 2; and the Greek subscripts $\alpha, \beta, \gamma, \delta$ take the value of 1, 2 or 3. If $\Delta(\cdot)$ denotes the difference between field variables $(\cdot)$ inside and outside the band, the inhomogeneous velocities within the shear band satisfy

$$\Delta v_i = f_i(n_k x_k, t). \tag{3.1}$$

Assuming that the inhomogeneous velocities do not vary along a shear band (Storen and Rice, 1975), the inhomogeneous deformation rate can be written as

$$\partial \Delta v_i / \partial x_j = n_j f_i', \tag{3.2}$$

where $f_i' = \partial f_i / \partial (n_k x_k)$. For the material subjected to multiaxial loading, the equilibrium conditions and their derivatives with respective to time are

$$\sigma_{\alpha\beta,\beta} - \rho \dot{v}_\beta = 0, \quad (\dot{\sigma}_{\alpha\beta,\beta} - \rho \ddot{v}_\alpha) + v_\gamma (\sigma_{\alpha\beta,\beta} - \rho \dot{v}_\alpha)_{,\gamma} = 0,$$

where comma indicates differentiation (*e.g.*, $\sigma_{\alpha\beta,\beta} = \partial \sigma_{\alpha\beta} / \partial x_\beta$). Therefore, the stress rates satisfy

$$\dot{\sigma}_{\alpha\beta,\beta} - \rho \ddot{v}_\alpha = 0. \tag{3.3}$$

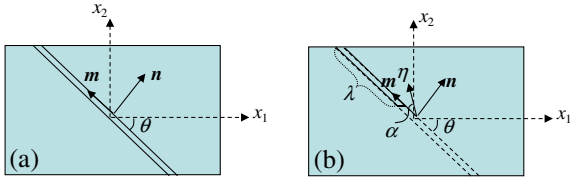

Fig. 3. Coordinate system and direction of the incipient shear band: (a) a shear band across the sample; and (b) the shear band propagating a distance λ.

Noting that Eqs. (2.7), (2.8) and (2.12) establish a series of linear algebra equations of $\dot{\sigma}_{\alpha\beta}$ and $v_{\gamma,\delta}$, the solution renders a relationship between the stress rate and the rate of deformation:

$$\dot{\sigma}_{\alpha\beta} = L_{\alpha\beta\gamma\delta} v_{\gamma,\delta}, \tag{3.4}$$

where $L_{\alpha\beta\gamma\delta}$ stands for the incremental tangent modulus tensor in the current (deformed) configuration. We leave out the lengthy expressions of $L_{\alpha\beta\gamma\delta}$ for the sake of brevity. One can obtain the solution by using any mathematics software. Applying Δ to both sides of Eq. (3.3) and substituting Eq. (3.4) into it will give rise to (note $\Delta v_3 = 0$)

$$(L_{ijkl} \Delta v_{k,l})_{,j} = \rho \Delta \ddot{v}_i. \tag{3.5}$$

It is noted that $\Delta L_{ijkl} = 0$ since L_{ijkl} is evaluated from the homogenous stress field right before bifurcation. Similarly, $\Delta \rho = 0$ since the material is initially homogenous and the density remains uniform right before bifurcation. If the stress and strain fields are uniform, we further have

$$L_{ijkl,j} = \frac{\partial L_{ijkl}}{\partial x_j} = \frac{\partial L_{ijkl}}{\partial \sigma_{mn}} \frac{\partial \sigma_{mn}}{\partial x_j} + \frac{\partial L_{ijkl}}{\partial \varepsilon_{mn}} \frac{\partial \varepsilon_{mn}}{\partial x_j} = 0. \tag{3.6}$$

Thus Eq. (3.5) reduces to

$$L_{ijkl} n_j n_l f_k'' = R_{ik} f_k'' = \rho \ddot{f}_i. \tag{3.7}$$

For the quasi-static deformation, the inertia terms $\rho \ddot{f}_i$ vanish. To have nontrivial solution of f_k'', the determinant of R_{ik} must vanish, namely

$$\|R_{ik}\| = 0. \tag{3.8}$$

For a dynamic case, suppose that R_{ik} is diagonalizable with two real eigenvalues $R_1, R_2 (R_2 > R_1)$. The corresponding eigenvectors are $\boldsymbol{\eta}$ and $\boldsymbol{\eta}'$, respectively. If $R_2 > R_1 > 0$, any nonzero velocity disturbances f_i will have components along $\boldsymbol{\eta}$ and $\boldsymbol{\eta}'$, propagating along $\boldsymbol{n}$ (the direction normal to the shear band) at velocities $\sqrt{R_1/\rho}$ and $\sqrt{R_2/\rho}$ respectively and vanishing at the boundary. Therefore, the critical condition for localization is $R_1 = 0$ (*i.e.* $\|R_{ik}\| = 0$), that is the velocity discontinuity along $\boldsymbol{\eta}$ is not propagative. It is noted that the velocity disturbance must emanate from a local deformation unit. Since the disturbance is not propagative along $\boldsymbol{n}$, the width of the shear band should equal the size of the deformation unit. The question is what the size of the deformation unit or the shear band is. According to Zhang and Greer (2006), there are several length scales in metallic glass: the atomic diameter is in the order of 0.21 to 0.31 nm; the size of the smallest atomic cluster, envisioned as the first-nearest-neighbor shells of solvent atoms around a central solute atom, is about 0.6 to 0.9 nm; while the shear band width, according to electron microscopy images, is about 10 nm. If the atomic cluster is considered as the fundamental building blocks of the material, the shear band should be about ten times the size of the fundamental building block, a relationship closely resembling that of the granular materials (Francois et al., 2002).

Since the velocity discontinuity along $\boldsymbol{\eta}$ does not propagate along $\boldsymbol{n}$, the propagation of a shear band can be accounted by assuming that the velocity field within the band satisfies

$$\Delta v_i = \eta_i g(\xi_n, \xi_m, t), \tag{3.9}$$

where

$$\xi_n = n_k x_k \quad \text{and} \quad \xi_m = m_k x_k.$$

Here the particle velocities within the shear band vary both in $\boldsymbol{n}$ and $\boldsymbol{m}$ directions. Fig. 3(b) illustrates the scenario of shear band propagation, in which the shear band emanating from the boundary has the length λ. $\boldsymbol{\eta}$ is not necessarily parallel to $\boldsymbol{m}$ since the deformation within the band is both shearing and dilating. The angle between $\boldsymbol{\eta}$

and $\boldsymbol{m}$ is denoted by α. It will be shown in Section 5 that the velocity of the shear band is related to α.

Substituting Eq. (3.9) into Eq. (3.5) yields

$$R_{ik}\eta_k g_{,nn} + L_{ijkl}m_j m_l \eta_k g_{,mm} + L_{ijkl}(n_j m_l + n_l m_j)\eta_k g_{,mn} = \rho \eta_i \ddot{g}, \quad (3.10)$$

where

$$g_{,nn} = \frac{\partial^2 g}{\partial \xi_n^2}, \quad g_{,mm} = \frac{\partial^2 g}{\partial \xi_m^2} \quad \text{and } g_{,mn} = \frac{\partial^2 g}{\partial \xi_m \partial \xi_n}.$$

As a possible solution of Eq. (3.10), we further assume that $g_{,mn} = 0$. Since $R_{ik}\eta_k = R_1\eta_k = 0$, multiplying η_i to both side of Eq. (3.10) yields

$$L_{ijkl}m_j m_l \eta_i \eta_k g_{,mm} = \rho \ddot{g}. \quad (3.11)$$

The velocity of shear band propagation is then

$$\dot{\lambda} = \sqrt{L_{ijkl}m_j m_l \eta_i \eta_k / \rho}. \quad (3.12)$$

4. Analytical solutions

4.1. Flow serration

For metallic glass with some compressive ductility, the load–displacement response exhibits many serrations. Each serration is a relaxation event associated with three critical phenomena: (i) the formation of shear bands, (ii) the quick increase of the inelastic shear strain within the shear bands, and (iii) the unloading outside the shear bands. After this relaxation, the material can resist further deformation, embodied by the increase of the reaction force until the occurrence of the next serration. Previous theories can demonstrate the deformation localization and the load drop by devising a mechanism for the prestigious drop of viscosity at a critical stress state, but not the mechanism of the subsequent local hardening. Our constitutive model can describe both the load drop and the hardening straightly.

Let us consider a simple shear case shown in Fig. 4(a), where a metallic glass sample of width L is subjected to shear stress τ. At a critical stress state, n shear bands of width b emanate. The successive material response within a shear band can be considered as the fast transformation from Points A to B in Fig. 4(b), where A is the bifurcation point. The work done associated with this local

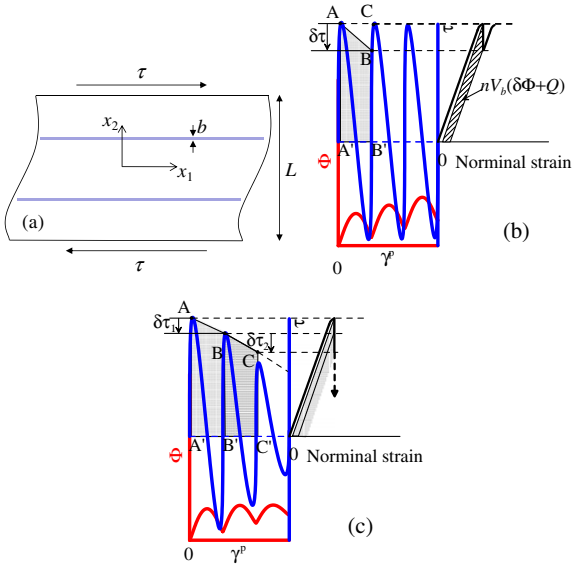

Fig. 4. (a) The simple shear deformation of a metallic glass sample, (b) the relation between macroscopic stress serration and microscopic stress instability in the shear band, and (c) the catastrophic failure.

strain burst is the combination of thermal dissipation Q and the free energy change $\delta\Phi$ (see Eq. (2.2)). Since the unloading outside the shear band is purely elastic, the decrease of the far-field shear stress is given by

$$\delta\tau = n\frac{(Q+\delta\Phi)}{\gamma_b^e}\frac{V_b}{V_s} = n\frac{b(Q+\delta\Phi)}{L\gamma_b^e}, \quad (4.1)$$

where V_b and V_s denote the volume of the shear band and the sample, respectively, and γ_b^e is the elastic strain at the bifurcation point. γ_b^e may also be considered as the strain at elastic limit (i.e., the yield strain), which can be a constant for most metallic glass (≈0.0267 according to Johnson and Samwer (2005)).

Fig. 4(b) schematically illustrates the relationship between macroscopic stress serration and microscopic shear transformation within shear bands. If A and C are the bifurcation points and if the far field stress τ drops linearly with local plastic strain development, the work done per unit volume within the shear band is the trapezoidal area ABB′A′, that is, $\int_0^{\gamma_0}\tau d\gamma^p = Q + \delta\Phi = (\tau_b + \delta\tau/2)\gamma_0$, where τ_b is the stress at the bifurcation point. Therefore, Eq. (4.1) becomes

$$\delta\tau = \frac{2\tau_b}{(1 + 2L\gamma_b^e/nb\gamma_0)} \approx \tau_b\frac{nb}{L}\frac{\gamma_0}{\gamma_b^e}, \quad (4.2)$$

when $L\gamma_b^e >> nb\gamma_0$. Eq. (4.2) reveals that the more shear bands form, the larger force drop takes place. For metallic glass with good compressive ductility, the material can evolve after a few serrations to a self-organized critical state (Sun et al., 2010; Wang et al., 2009a), at which a larger number of shear bands formed with the consequence of a larger force drop. At this moment the overall material can relax at the lower stress, increasing the probability to fracture at a large plastic strain. Providing that the width of shear band is the intrinsic length parameter of amorphous metals, Eq. (4.2) indicates that the force drop tends to increase as the specimen size reduces. As an example, for the zirconium-based BMG, the magnitude of force drop is within 2% of the average flow stress for the specimen in millimeter scale (Wang et al., 2009a), while about 8–10% for the specimen of several micrometers (Ye et al., 2010). The magnitude of the force drop does not scale linearly with the specimen size since the number of shear bands also decreases as the specimen size reduces.

After force drops, the deformation units within the shear band regain the hardening ability, which is indicated by the stress increase from Point B to the next bifurcation point C, as shown in Fig. 4(b). In the process from B to C, the shear band heals up and the material can resume the homogenous deformation until it reaches the next bifurcation point. This is the fundamental process underpinning the serrations of the stress–strain curve of metallic glass. It is also the fundamental cause of the good compressive ductility of some types of metallic glass. In these materials, the shear bands can heal up and do not develop to the catastrophic band. However, in a different scenario, as schematically shown in Fig. 4(c), the material within the shear bands may be significantly deteriorated by the plastic deformation, and the force drop $\delta\tau$ may be too small for the material to recover. Catastrophic failure then occurs. In this case, Points B and C are still higher than the bifurcation points, such that the deformation continuously localizes within shear bands, leading to the catastrophic failure.

4.2. Shear band angle

Uniaxial compression and tension tests are the most common experiments in the characterization of mechanical properties and shear banding of metallic glass. Therefore, as the application of our new constitutive model, let us investigate the solutions of Eq. (3.8) for understanding the deformation of metallic glass under such loading conditions. We assume that shear band forms at the

critical uniaxial stress σ_0 to accommodate plastic deformation. Mukai et al. (2002) found the small jumps in the stress–strain curve before the macroscopic yielding point and concluded that shear band may emanate prior to macroscopic yielding. Their observation implies that a BMG may have weaker regions with lower yielding stress than the macroscopic one. Therefore the critical stress σ_0 may be slightly smaller than the macroscopic yield stress. But for simplicity, we let σ_0 equals to the macroscopic yielding stress.

Three loading conditions, namely the plane strain, axisymmetry and plane stress are considered. The solutions are presented in the Appendix and the relationships between the diltancy factor β and the shear band inclination angle θ are summarized in Fig. 5(a). Owing to the small difference in the tensile and compressive strength of metallic glass (Table 1), which implies a small μ, we conjecture that the large diversity of shear band inclination angles (Zhang et al., 2003b) is mainly caused by the variation of the dilatancy factor β. Fig. 5(a) shows that a larger β leads to larger deviation from 45°, that the shear band angle differs remarkably at different loading conditions, and that plane-stress tension gives maximum shear band angle. If β is sufficiently large (>2), the shear band can be perpendicular to the loading direction for uniaxial tension or in parallel with it for uniaxial compression, as have been observed in experiments (Zhang et al., 2003b).

Fig. 5(b) shows the relationships between $h/|\sigma_0|$ and θ at the bifurcation point. For the three loading conditions shown in Fig. 5(b), it seems that a larger ductility can be achieved most easily when compressing an axisymmetric specimen, as the hardening rate h at the bifurcation point is the most negative in this case. A negative h indicates that the bifurcation point, *e.g.*, A′ in Fig. 5(c), is on the downhill part of stress–strain curve. After the bifurcation, the local deformation within the shear band renders the force drop and turns the stress state to Point B, which is on the uphill part. If the next bifurcation point is C′, it is evident that a more negative h will lead to a larger distance between B and C′. This distance is the overall strain required to invoke a second bifurcation. From B to C′, the material deforms homogenously and the shear band heals up. Therefore, a more negative h implies a less probability for a shear band to develop to a catastrophic band. Nevertheless, it also implies that the metallic glass may be ductile under one stress state but becomes brittle under another owing to the different bifurcation point under different stress state.

4.3. Spreading speed of shear banding instability

Shear banding instability propagates as the global stress state reaches a bifurcation point, at which a local excessive shear transformation triggers a chain process of atomic rearrangement along the most preferable direction (direction of maximum h) that eventually organizes the shear band. At the same time, this inelastic shear displacement reduces the possibility of instability in adjacent regions, by relieving the elastic strain energy of regions outside the shear band. Therefore the shear band is usually sharply localized. The instability propagating speed can be evaluated from Eq. (3.12). Fig. 6 shows the relation between the normalized shear band extension speed $\dot{\lambda}/c_s$and the shear band inclination angle θ for the cases of plane-strain compression and tension, where $c_s = \sqrt{G/\rho}$ is the shear wave speed and $c_d = \sqrt{(K + 4G/3)/\rho}$ is the dilatation wave speed. It is noted that the shear band extends at the speed between the shear wave speed and dilatation wave speed. The fastest instability (at the speed of c_d) occurs as the propagation path inclines exactly at 45°. The subsonic shear band ($\dot{\lambda} < c_s$) occurs only when the diltancy factor is very large ($\beta > 1.9$) and when the shear band inclination angle differs considerably from 45°. The variation of $\cos\alpha$ is plotted in Fig. 6. If $\cos\alpha = 1$, the shear band extends at c_d. In this case, the local velocity disturbance is in parallel with the shear band, which makes the instability propagates in the same way as a dilatation wave does. If $\cos\alpha = 0$, which resembles the scenario of a shear wave propagation, the shear band extends at the velocity slightly smaller than c_s. Although the above observation is under the plane-strain compression/tension, the same conclusion is applicable to other stress states according to our calculation.

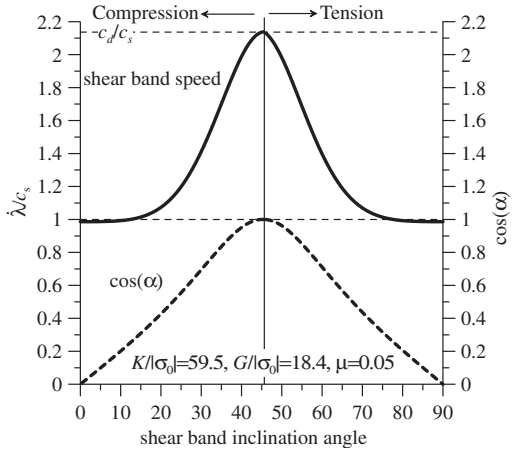

Fig. 6. The velocity of shear band extension for the plane-strain case.

It should be noted that the intersonic shear banding instability is not reported in literature. In almost all investigations, people

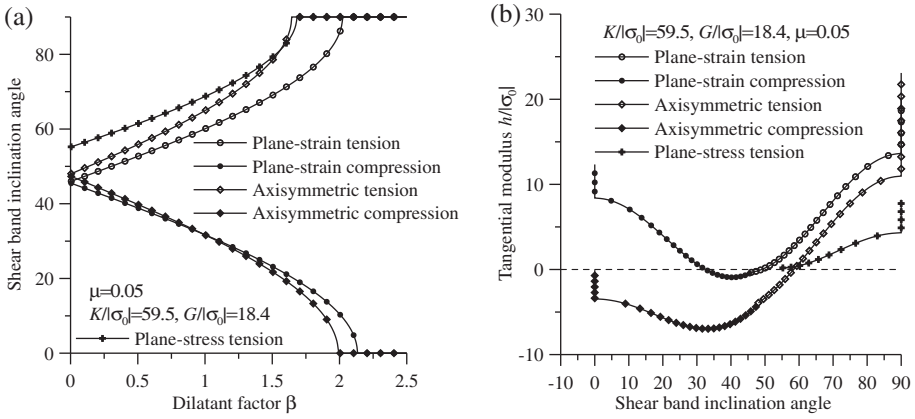

Fig. 5. (a) The relationships between dilatancy factor β and the shear band inclination angle θ; (b) the relationships between shear band inclination angle θ and hardening rate h at bifurcation point.

assumed that the shear band speed is bounded by the shear wave speed. Molecular dynamic simulations (Cao et al., 2009) revealed that the propagation of severe atomic structure disordering is approximately in the speed of shear wave. However, the intersonic instability propagation, revealed in our calculation, is not the propagation of sever plastic deformation but just the transmission of a velocity disturbance along a particular path in the solid. Therefore, in a molecular dynamic simulation, the propagation of instability should be embodied by the sequentially "displacement jump" of atoms along the particular band prior to the severe structural disordering. Cao et al. (2009) made the observation that before a shear band matures, the displacement jumps in the six different sites along this band occur almost simultaneously, much faster than the shear wave propagation. Since any mechanical disturbance transmitting in solid cannot be faster than the dilatation wave, the observation of Cao et al. (2009) corroborates that the propagation of the shear banding instability is intersonic.

5. Finite element simulation

To investigate the deformation of metallic glass under more complex loading conditions, numerical analysis is necessary. We use the commercial FEM code ABAQUS EXPLICIT to simulate the dynamic response of metallic glass. The constitutive model is implemented as a user material subroutine (VUMAT). The Φ–γ^p relation is assumed to be

$$\Phi(\gamma^p) = \varphi_0 \sin^4(\pi\gamma/\gamma_0) f_d(\varepsilon_v) + \varphi_\alpha \sin^2(\pi(\gamma^p + \zeta)/\gamma_\alpha), \tag{5.1}$$

$$\gamma^p = \gamma' - \frac{\gamma_0}{2\pi} \sin\left(\frac{2\pi\gamma'}{\gamma_0}\right). \tag{5.2}$$

where γ' is the internal deformation variable representing the total atomic strain (Rice, 1992), φ_0 is the local energy barrier for the atomic jump from one basin to the adjacent one; $\pi\varphi_0/\gamma_0$ is the peak resistance to plastic deformation of the material; φ_α and γ_α pertain to the α-relaxation of glass, ζ represents the initial state of the local atomic cluster which could be in a random energy basin in the free energy landscape. φ_α, γ_α and ζ are used to reflect the fact that different arrangements of atoms are in the different basins of the free energy landscape and that an amorphous solid is an ensemble of many different atomic structures. $f_d(\varepsilon_v)$ is a decay function which describes the dilatation induced structural softening. We set

$$f_d(\varepsilon_v) = \begin{cases} \exp\left[-(C(\varepsilon_v - \varepsilon_{v0})/\xi_0)^m\right], & \varepsilon_v > \varepsilon_{v0} \\ 1, & \varepsilon_v \leqslant \varepsilon_{v0} \end{cases}. \tag{5.3}$$

The above equation implies that the atomic system is not softened until the total volumetric strain reaches the threshold value ε_{v0}.

Eqs. (5.1)–(5.3) are purely phenomenological, which aims to use minimum number of parameters to describe the rugged free energy landscape. Referring to the Zirconium-based metallic glass (Jiang and Dai, 2009), the parameters used in simulations are given in Table 2. The intention of conducting simulations with these parameters is not to quantitatively compare the numerical result with a specific experiment but just use the numerical tool to study the deformation mechanism of metallic glass. Nevertheless, it should not be difficult to match the simulation result, by tuning these parameters, with a specific experimental result in terms of strength and ductility.

5.1. Plain-strain compression and tension

Fig. 7(a) shows tensile and compressive true stress–strain curves obtained under different strain rates. The numerical model is a 6 × 12 mm plane-strain block, discretized with 50 × 50 μm 4-node quad elements. The serrations of the stress–strain curve are revealed in the inset. It is noted that the model material have notable ductility in the compression test when the strain rate is 0.1 s^{-1} and 1 s^{-1}. In contrast, the tensile ductility is almost zero. This difference is attributed to the fact that the compressive force tends to suppress the dilatation, deferring the material weakening.

Table 2
The parameters used in finite element simulations.

Symbols	Unit	Value
$\pi\varphi_0/\gamma_0$	GPa	1.0
γ_0		0.01
φ_α/φ_0		1
γ_α/γ_0		50
ζ/γ_0		Random number between 0–20
C		0.2
ε_{v0}		0.0075
m		1.5
μ		0.05
β		0.1
τ_0	MPa	50
$\dot{\gamma}_0$	s^{-1}	1
K	GPa	114.3
G	GPa	35.3
ρ	kg m^{-3}	6125
Thermal conductivity	W m^{-1} K^{-1}	20
Specific heat	J kg^{-1} K^{-1}	400

Under different strain rates, the initial yield stresses differs negligibly, indicating very weak rate sensitivity, which is consistent with experimental findings (Schuh et al., 2007). After the initial yield point, a sudden drop of the flow stress occurs and the successive flow stress is smaller than the initial yield stress. This phenomenon is not observed in metallic glasses but is akin to the stress–strain curves of those well annealed metals (*e.g.*, iron) which exhibit upper and lower yield points. In our simulation result, the initial yield point is corresponding to the peak resistance to the plastic deformation (point *P* in Fig. 1(c)), while the successive local peaks of the serrated flow stress are the stresses at the bifurcation points (say points A, C or A′, C′ in Fig. 1(c)). In reality, the peak resistance to the plastic deformation is hardly captured since the real materials are always inhomogeneous and have residual stresses inherited from manufacturing process. This initial inhomogeneity can lead to early plastic deformation before macroscopic yielding as experimentally observed by Mukai et al. (2002). However, in the simulation we assumed the ideally annealed material, i.e., the initial free energy of every deformation unit is in the local minimum. Therefore, a sufficient number of deformation units reach the peak resistance simultaneously, giving rise to significant drop of the stress due to the bursts of plastic deformation afterwards in many regions. Such phenomenon can be mitigated by increasing the inhomogeneity of the simulation model. We increase φ_α/φ_0 from 1 to 10, such that the deformation units initialized at different free energy minimums (characterized by ζ) have more significant difference in the resistance to the plastic strain. Fig. 7(b) plots the resulted stress–strain curve. It is noted that the yielding point is less distinct. The transition from elastic to elastoplastic deformation is continuous and smooth.

Fig. 7(c) shows that at the same compressive strain level (engineering strain = 1.8%), higher strain rate leads to more shear bands, which is consistent with experimental findings (*e.g.*, Liu et al., 2005). More shear bands tend to toughen the metallic glass and result in better ductility as revealed in Fig. 7(a). The transient temperature change due to the plastic dissipation within shear bands is also considered. The snapshots are shown in Fig. 5(d), which are taken at the same strain level as that of Fig. 7(c). The temperature rise (from the room temperature 293 K) is merely a few degrees, which therefore should not be considered to be the major cause of the shear band formation.

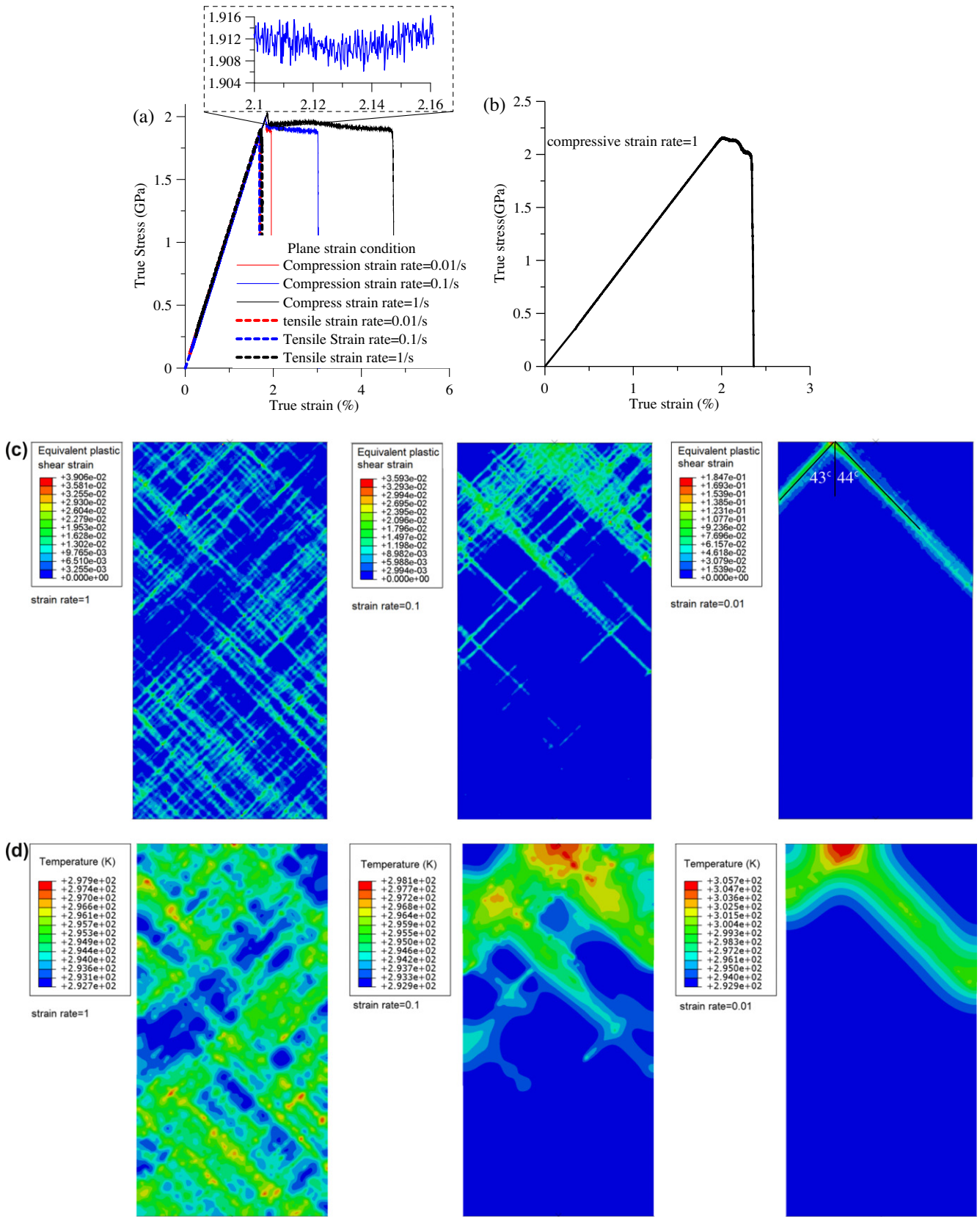

Fig. 7. Plane-strain tension and comparison: (a) the stress–strain curves; (b) the compressive stress–strain curve of the material with larger inhomogeneity; (c) the shear band morphologies resulted from different strain rates at 1.8% engineering strain; and (d) the temperature profiles around the shear bands at 1.8% engineering strain.

5.2. Two-phase model

For the quasi-static compression (strain rate = 0.01), merely a single shear band forms after the yielding point (shown in Fig. 7(c)) and the ductility is vanishingly small as shown in Fig. 7(a). However, many as-cast metallic glasses have very good compressive ductility under the quasi-static condition. The most exceptional one is reported by Liu et al. (2007). They ascribed the good ductility to the coexistence of hard and soft phases, which were observed in the electron microscopy images .(Liu et al., 2007) and detected by nano-indentation (Wang et al., 2009b). We can test their conjecture in our simulation model. Suppose that the harder phase, namely phase II, possessing 20% larger peak resistance (all the other parameter is identical to phase I), is randomly blended with the phase I as shown in Fig. 8(a). Fig. 8(b) shows the tensile curves of the monolithic BMG and the two-phase mixtures under quasi-static compressions, where f_{II} is the volume fraction of phase II. The result clearly indicates that the coexistence of hard and soft metallic glass phases, although both brittle, can notably improve the compressive ductility of the composite, corroborating the conjecture of Liu et al. (2007). It is interesting to note that both cases $f_{II} = 0.3$ and 0.7 are less ductile than $f_{II} = 0.5$, implying that either brittle phase taking the major fraction reduces the ductility. Fig. 8(c) shows that the enhancement of ductility is also owing to the increased number of shear bands.

5.3. Shear band inclination angle

Fig. 9(a) and (b) show the tensile stress–strain curves and the shear band morphologies, respectively, corresponding to the three stress states discussed in Section 4.2. For the case of a $12 \times 6 \times 0.2$ mm thin BMG sheet the shear band inclination angle is 58°, which is in reasonably good agreement with the analytical calculation (56°). We assumed in Appendix A.3 that for the very thin specimen the bifurcation condition should incorporate the variation of the thickness. This consideration has been validated herein. The shear band angles of the plan-strain model and the cylindrical model under tensile loadings are 49° and 51°, respectively, only slightly larger than those of theoretical calculation (47° and 50° for plane-strain and axisymmetrical cases, respectively). From these simulations, we may conclude that the finite element result has verified our analytical calculations in Section 4.2. The slight deviation may be attributed to the mesh fineness and large deformation.

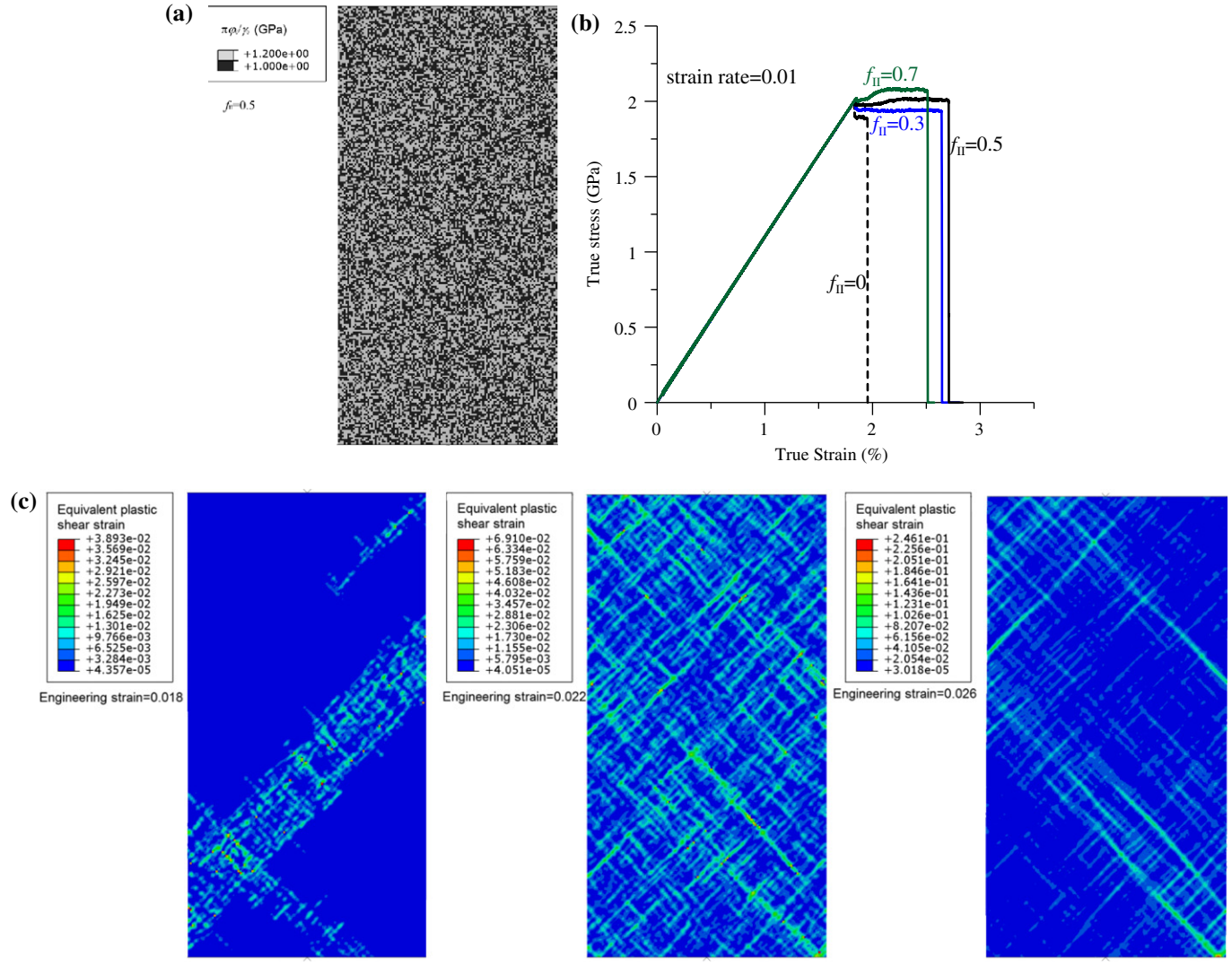

Fig. 8. The deformation of 2-phase metallic glasses: (a) the initial random distribution of the two phases; (b) the stress–strain curves for different volume fractions of phase II; and (c) the consecutive snapshots of shear band morphologies for the case of $f_{II} = 0.5$.

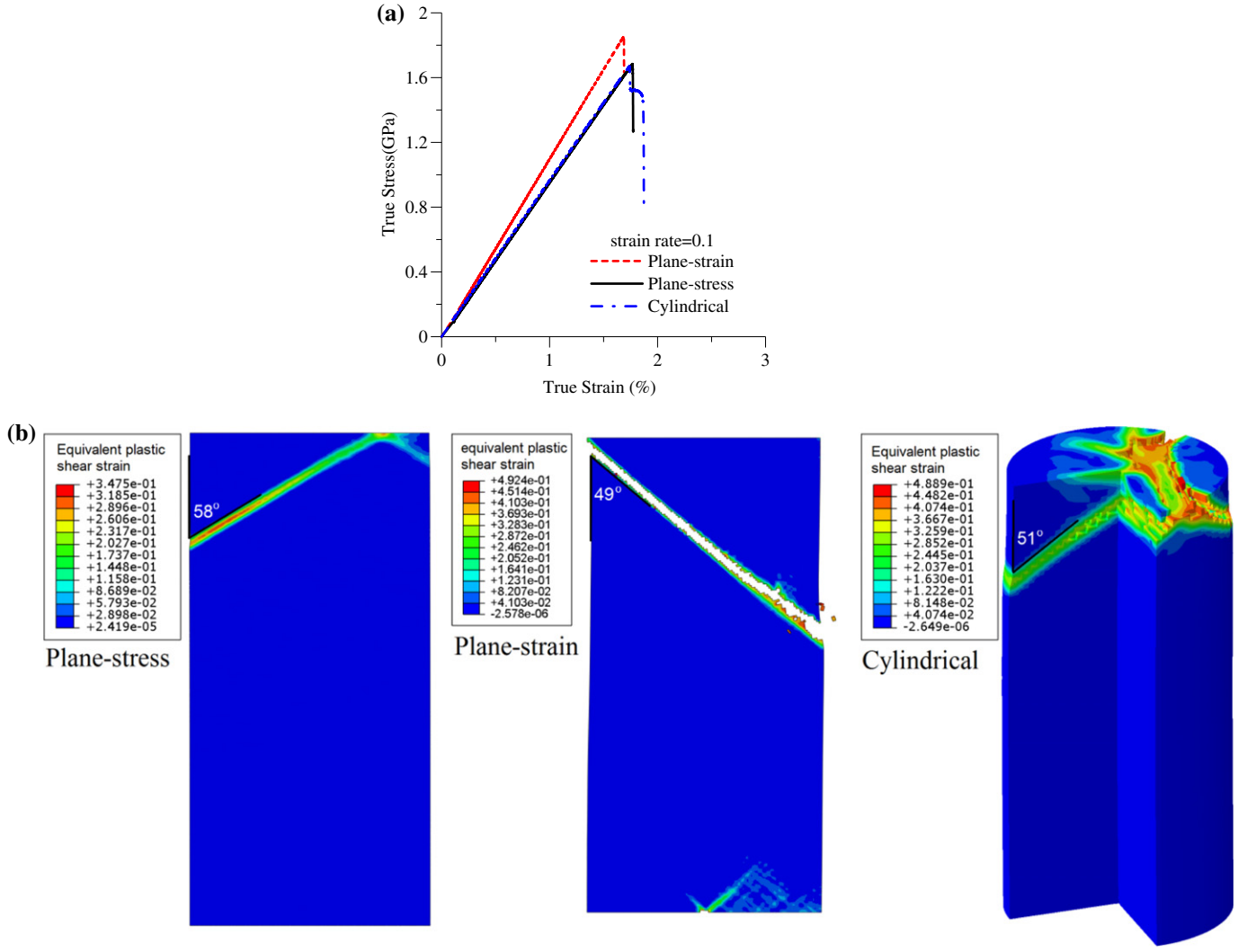

Fig. 9. The tensile deformation of metallic glass under different conditions: (a) the stress–strain curves and (b) the shear band inclination angles a thin sheet, the plain-strain and cylindrical models.

5.4. Geometric effect on ductility

It is noted that in Fig. 9(a) the cylindrical model exhibits some tensile plasticity, while the other two models fracture right after the yielding point. We inferred in Section 4.2 that the axisymmetric stress field should render the more ductility than the plane-strain case based on the position of the bifurcation point. This inference can be validated by numerical simulations. Fig. 10 compares the stress–strain curves resulted from the quasi-statically compressed plane-strain model and the cylindrical model. We used the 4-node quad element for the plane-strain model and the 8-node brick element with reduced integration point for the cylindrical model. The mesh sizes are both 50 μm. Both models were compressed by a rigid plate at an engineering strain rate 0.01 s^{-1}. The comparison of the stress–strain curves exhibits that the cylindrical specimen has much larger ductility than the plain-strain one. Hence, we shall remark that it is easier to obtain good ductility when compressing a cylindrical BMG specimen. However the material may be brittle in other geometry or stress state. It is worth noting that in literatures almost all metallic glasses possessing high compressive ductility were tested in the cylindrical form.

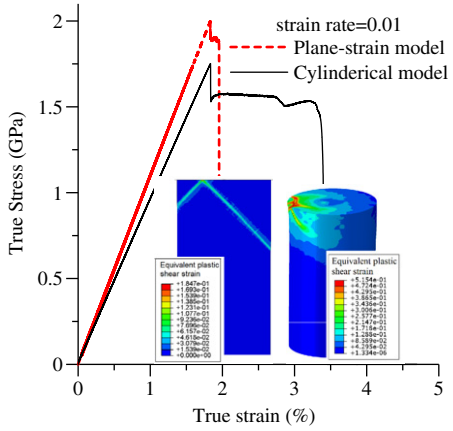

Fig. 10. The compressive deformations of metallic glasses under plane-strain condition and in cylindrical form.

5.5. Cylindrical indentation

In addition to tension and compression, indentation is also frequently used to study the mechanical properties of BMG. In this

case, the deformation of materials under the indenter is constrained, which allows stable development of multiple shear bands and avoids unstable failure. Berkovich or Vickers indentation on BMG was studied in many works, which has been reviewed by Schuh and Nieh (2004). However, in these indentations, the development of shear bands inside the material is difficult to observe. Although the bonded-interface method was used to resolve this problem, this method causes the different stress/strain field from that of the pristine material (Helbawi et al., 2001). An alternative choice is the 2D cylindrical indentation, which allows directly observation of shear bands in the polished surface. This method has been chosen by Su and Anand (2006b), Antoniou et al. (2007) and others. We shall simulate the cylindrical indentation with our constitutive model. Another reason for studying 2D indentation is that in 2D case the numerical model can be meshed with very small elements such that the fine deformation pattern can be resolved. However, in 3D case, to resolve the fine shear bands, the number of elements must be millions and simulation will take too long time even with a high-performance computation system.

Fig. 11(a) shows the simulation model. The cylindrical indenter is rigid with radius 2.4 mm and 0.8 mm as were used by Antoniou et al. (2007). The smallest element beneath the indenter is of 5 μm. It should be reminded that typical shear band thickness is tens of nanometers. Therefore the shear bands can be better shown in

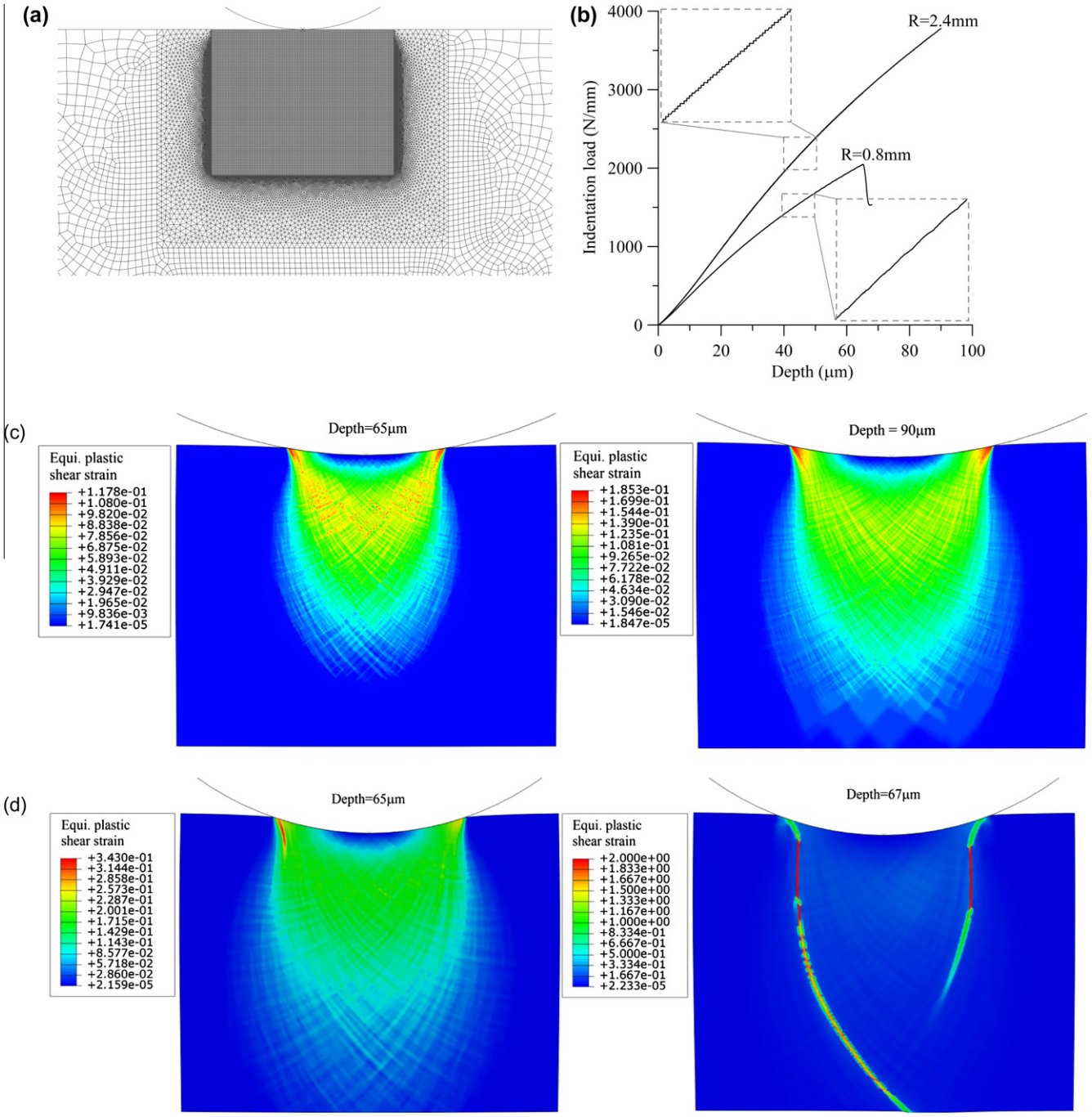

Fig. 11. Cylindrical indentations: (a) the FE model; (b) the load-depth curves and (c, d) the contour plots of equivalent plastic shear strain for (c) 2.4 mm indenter and (d) 0.8 mm indenter.

simulation if the element size is reduced to nanoscale. However, due to the limitation of computation, we have to use larger element and the shear band cannot be as thin as experiment. Furthermore, to save the computational time in the explicit simulation, we used a much faster indenting speed 100 μm/s than that was adopted by Antoniou et al. (2007) in the experiment (1 μm/s). Such a high deformation rate causes the pop-ins of the load-deformation curve less pronounced (Schuh and Nieh, 2004). But the morphology of the equivalent plastic shear strain has been very similar to the experimental result. Fig. 11(b) shows the load-displacement curves for 2.4 mm and 0.8 mm cylindrical indenter. The enlarged portions shown in the insets demonstrate small pop-ins. It is interesting to note that at the same range of indentation depth, the pop-in for the case of 2.4 mm is very different from that for the case of 0.8 mm, which however cannot be confirmed from experiments. We believe that these pop-ins are not numerical noises since they only occur as the indentation depth larger than 20 μm, where the sudden bust of plastic deformation within some shear bands becomes the main deformation process. Fig. 11(c) show the contour plots of the equivalent plastic shear strain at two indentation depths (65 μm and 90 μm) for the case of 2.4 mm cylindrical indenter. It is observed that two sets of curved shear bands emanate from the edges of contact region and proliferate with the increase of contact area, which agrees reasonably well with the experimental observations made by Antoniou et al. (2007).

For the case of 0.8 mm, as the indentation depth is larger than 65 μm, severe load drop occurs corresponding to the major shear bands shown in Fig. 11(d). Such significant load drop in simulation is because of the presumed decay function defined by Eq. (5.3), which assumes that a large dilation resulted from a large shear strain (say 100%) can leads to significant reduction of the strength (less than 1%). In cylindrical indentation experiments conducted by Antoniou et al. (2007) and Su and Anand (2006), such significant load drop is not observed. To match the experimental result, a simple way is to modify the decay function (Eq. (5.3)) to allow the simulation of cylindrical indentation continues to a larger depth without significant load drop. However, it is more important to point out that such difference implies that the confinement of surrounding materials, or particularly the hydrostatic pressure exerted by the surrounding materials, may play a significant role in preventing the material from significant deterioration at large shear strain, which needs further detailed investigation.

6. Conclusion

This paper has investigated the physical origin of shear bands in metallic glass by incorporating the fact that instability is due to the bifurcation of the constitutive model at a particular stress state. Unlike previous studies, the new constitutive model is established based on the rugged free-energy landscape of metallic glass, which naturally leads to the rate-insensitivity and flow serrations. The formulae for describing the nucleation and propagation of shear banding instability have also been developed. The study has brought about the following conclusions:

(1) Deformation localization in metallic glass is inevitable due to the rugged free energy landscape. A shear band, once emanated from a deformation unit, does not increase its thickness.
(2) The shear band angle is exactly the angle between the plane of instability and loading direction. The angle variation is significantly influenced by the diltancy factor β and pressure sensitivity μ.
(3) The theoretical speed of the shear banding instability varies between the dilatation wave speed and a speed slightly smaller than the shear wave speed.
(4) Our finite element simulation shows that the new constitutive model predicts well what has been observed in experiments, *i.e.*, (a) more shear bands can toughen the metallic glass, leading to a higher ductility; (b) higher strain rate gives rise to more shear bands; (c) the introduction of a harder (or softer) phases does improve the ductility; and (e) the ductility depends on the sample geometry or the stress state.

Acknowledgements

This work was supported by the Australian Research Council. The finite element simulation was run on the HPC in National Computational Infrastructure of Australia. We are grateful for their support.

Appendix A

A.1. Plane-strain

Under plane-strain deformation, the components of the stress tensor prior to bifurcation are given by

$$\sigma_{13}=\sigma_{23}=0 \quad \text{and } \sigma_{33}=\nu(\sigma_{11}+\sigma_{22}), \quad \sigma_{11}=\sigma_0,$$
$$\sigma_{22}=0, \quad \sigma_{33}=\nu\sigma_0, \quad \sigma_{12}=0,$$

where ν is Poisson's ratio. The equivalent shear stress is $\bar{\tau}=|\sigma_0|\sqrt{(1+\nu^2+(1-\nu)^2)/6}$. Solving Eq. (3.8) yields

$$h(\theta)/|\sigma_0| = \frac{\begin{array}{l} 2\overline{G}^2(7-16\nu-8\nu^2)+2\overline{G}\overline{K}(5-8\nu+8\nu^2)-6\overline{K}(\beta+2\mu)\bar{\tau}/|\sigma_0| \\ -\overline{G}(7-14\nu+8\nu^2)\sigma_0/|\sigma_0|+16\overline{G}\overline{K}((\beta+\mu)(1+\nu))\bar{\tau}/\sigma_0+64\overline{G}\overline{K}\beta\mu\bar{\tau}^2/\sigma_0^2 \\ +\overline{K}\left(2(1-2\nu+\nu^2)+(\beta+\mu)(2\nu-1)\bar{\tau}/\sigma_0+8\beta\mu\bar{\tau}^2/\sigma_0^2\right)\cos 2\theta \\ +\left(2\overline{G}^2+6\overline{G}\overline{K}-\overline{G}\sigma_0/|\sigma_0|+2\overline{G}\nu\sigma_0/|\sigma_0|-6K\beta\bar{\tau}/|\sigma_0|\right)\cos 4\theta \end{array}}{8\left(4+3\overline{K}/\overline{G}\right)(\tau^2/\sigma_0^2)\left(2\overline{G}-\sigma_0/|\sigma_0|\cos 2\theta\right)}, \tag{A.1}$$

where

$$\overline{K}=K/|\sigma_0| \quad \text{and } \overline{G}=G/|\sigma_0|.$$

For Zirconium-based metallic glass ($Zr_{41.2}Ti_{13.8}Cu_{10}Ni_{12.5}Be_{22.5}$, $\nu=0.36$), $\overline{K}=59.5$ and $\overline{G}=18.4$ (Jiang and Dai, 2009). Fig. A1 shows the variation of $h/|\sigma_0|$ with θ. It is clear that μ and β affect the shear band inclination angle in a similar way.

A.2. Axisymmetry

For an axisymmetric compression or tension, the homogenous stress field prior to bifurcation is

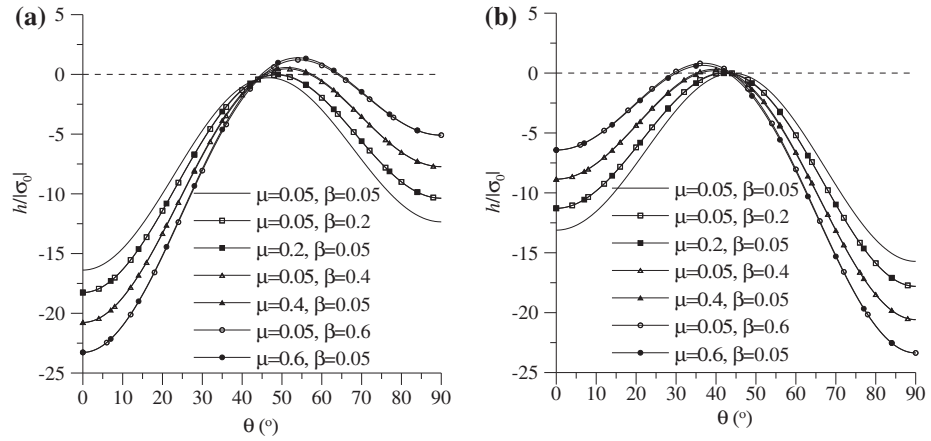

Fig. A1. $h/|\sigma_0|$-θ curves under plane-strain condition: (a) unixial tension and (b) uniaxial compression.

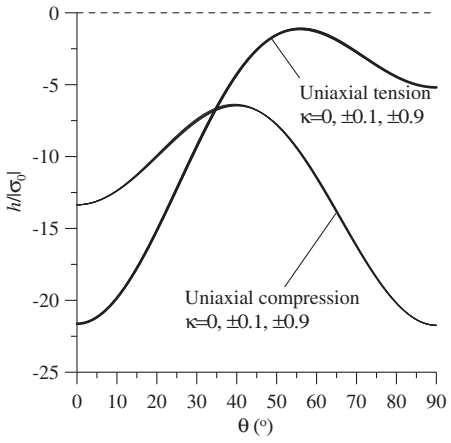

Fig. A2. Effect of confinement stress on $h/|\sigma_0| - \theta$ curves obtained under axisymmetric condition.

$$\sigma_{11} = \sigma_0, \quad \sigma_{22} = \sigma_{33} = \kappa\sigma_0, \quad \sigma_{12} = \sigma_{13} = \sigma_{23} = 0,$$
$$\bar{\tau} = (1-\kappa)|\sigma_0|/\sqrt{3} \quad \text{and } \kappa < 1,$$

where κ represents the ratio of the radial and circumferential confinement stresses to the axial stress due to the application of hydrostatic pressure (Lewandowski and Lowhaphandu, 2002) or the sleeves (Lu and Ravichandran, 2003). Solving Eq. (3.8) yields

$$h(\theta,\kappa)/|\sigma_0| = \frac{-\begin{pmatrix} 12(2\overline{G}^2 - (\overline{G}+2\overline{K})(1-\kappa)\sigma_0/|\sigma_0|)\cos 2\theta \\ +3\overline{G}\left(6\overline{G}+10\overline{K}-3(1-\kappa)\sigma_0/|\sigma_0| + \left(2\overline{G}+6\overline{K}+1-\kappa\right)\sigma_0/|\sigma_0|\right)\cos 4\theta \\ +8\sqrt{3\overline{G}\overline{K}}\sigma_0/|\sigma_0|(3\cos 2\theta - 1)(\beta+\mu) \\ +2\sqrt{3\overline{K}}(1-\kappa)(-3(2\mu+\beta)+2(\beta+\mu)\cos 2\theta - 3\beta\cos 4\theta) \end{pmatrix}}{8(4+3\overline{K}/\overline{G})(2\overline{G}-\sigma_0/|\sigma_0|(1-\kappa)\cos 2\theta)} + \frac{4\overline{K}\beta\mu}{4+3\overline{K}/\overline{G}} \tag{A.2}$$

Although Eq. (A.2) includes κ, we can see that the effect of κ on the $h/|\sigma_0| - \theta$ relationship is negligible, as demonstrated in Fig. A2. The overlapping of the curves indicates that the shear band inclination angles, corresponding to the maximum h in the curves, are insensitive to κ. Experimental investigations have indeed confirmed this finding. Lu and Ravichandran (2003) used the sleeve to confine the radial expansion of metallic glass. In their experiment, κ varied from 0.1 to 0.4 but the shear band inclination angle was always 45°. Lewandowski and Lowhaphandu (2002) tested metallic glass in pressurized chamber with κ from −0.35 to −0.03 for their tensile tests and from 0.15 to 0.3 for their compressive tests. They identified that the fracture angles were 57.5° ± 1.5° in pressurized tension and 40° in pressurized compression, irrespective of the κ variation.

A.3. Plane-stress

When a thin sheet of metallic glass is subjected to tension, the homogenous stress field prior to bifurcation is

$$\sigma_{11} = \sigma_0 > 0, \quad \sigma_{22} = \sigma_{33} = 0, \quad \sigma_{12} = \sigma_{13} = \sigma_{23} = 0, \quad \text{and}$$
$$\bar{\tau} = \sigma_0/\sqrt{3}.$$

This stress-field is identical to that of the axisymmetric tension with $\kappa = 0$. If only the stress state is considered, the shear band inclination angle of a very thin specimen should be identical to an axisymmetric case. However, due to the small thickness, the variation of the thickness caused by the inhomogeneous deformation becomes significant. Similar to Storen and Rice (1975), we shall incorporate the effect of the strain rate $\dot{\varepsilon}_{33}$ into consideration. Note that the in-plane forces and their changing rate satisfy

$$(H\sigma_{ij})_{,j} = 0, \quad \text{and } (\dot{H}\sigma_{ij} + H\dot{\sigma}_{ij})_{,j} + \nu_\alpha (H\sigma_{ij})_{,j\alpha} = (\dot{H}\sigma_{ij} + H\dot{\sigma}_{ij})_{,j} = 0.$$

By applying operator Δ (refer to Part I, Section 3) to the stress rate and the strain rate, we get

$$(\Delta\dot{\sigma}_{ij} + \sigma_{ij}\Delta(\dot{H}/H))_{,j} = (\Delta\dot{\sigma}_{ij} + \sigma_{ij}\Delta\dot{\varepsilon}_{33})_{,j} = 0. \tag{A.3}$$

Assuming that the volumetric strain rate remains continuous across the shear band boundary, we have

$$\Delta\dot{\varepsilon}_{33} = -(\Delta\dot{\varepsilon}_{11} + \Delta\dot{\varepsilon}_{22}) = -\left(n_1 f_1' + n_2 f_2'\right). \tag{A.4}$$

Substituting Eqs. (A.4) and (3.4) into Eq. (A.3) leads to

$$(L_{ijkl}n_jn_l - \sigma_{ij}n_jn_k)f'_k = 0. \tag{A.5}$$

The nontrivial solution of f'_k requires

$$\|L_{ijkl}n_jn_l - \sigma_{ij}n_jn_k\| = 0. \tag{A.6}$$

Solving Eq. (A.6) yields

$$h/|\sigma_o| = -\frac{\begin{pmatrix} 16\overline{K}\beta\mu(4\overline{G}^2 - 2\overline{G} - 1 + \cos 2\theta) + \\ 4\sqrt{3\overline{K}}(\beta+\mu)(4\overline{G}^2 - 8\overline{G} - 1 + b(12\overline{G}^2+1)\cos 2\theta) + \\ 66\overline{G}^2\overline{K} - 12\overline{G}^2 - 51\overline{G}\overline{K} - 12\overline{G} - 12\overline{K} + \\ 12(\overline{K} + \overline{G}(-3\overline{K}+1) + 6\overline{G}^2(3\overline{K}+1))\cos 2\theta \\ +3\overline{G}(18\overline{G}\overline{K} - 4\overline{G} - 3\overline{K})\cos 4\theta \end{pmatrix}}{4(16\overline{G}^2 + 8\overline{G}(6\overline{K}-1) - 6\overline{K} - 4 - 3\overline{K}/\overline{G} + (-18\overline{K} + 4 + 3\overline{K}/\overline{G})\cos 2\theta)}. \tag{A.7}$$

The consideration of the effect of strain rate $\dot{\varepsilon}_{33}$ makes the shear band inclination angle differs significantly from an axisymmetric case, as shown in Fig. 5(a). For example, if $\mu = 0.05, \beta = 0.1$, the shear band inclination angle is 56° for a plane-stress case and 50° for an axisymmetric case.

References

Anand, L., Su, C., 2005. A theory for amorphous viscoplastic materials undergoing finite deformations, with application to metallic glasses. Journal of the Mechanics and Physics of Solids 53, 1362–1396.

Antoniou, A., Bastawros, A., Biner, B., 2007. Experimental observations of deformation behavior of bulk metallic glasses during wedge-like cylindrical indentation. Journal of Materials Research 22, 514–524.

Argon, A.S., 1979. Plastic deformation in metallic glasses. Acta Metallurgica 27, 47–58.

Cao, A.J., Cheng, Y.Q., Ma, E., 2009. Structural processes that initiate shear localization in metallic glass. Acta Materialia 57, 5146–5155.

Dimiduk, D.M., Woodward, C., LeSar, R., Uchic, M.D., 2006. Scale-free Intermittent flow in crystal plasticity. Science 312, 1188–1190.

Eyring, H., 1936. Viscosity, plasticity, and diffusion as examples of absolute reaction rates. Journal of Chemical Physics 4, 283–291.

Francois, B., Lacombe, F., Herrmann, H.J., 2002. Finite width of shear zones. Physical Review E 65, 031311.

Gao, Y.F., Yang, B., Nieh, T.G., 2007. Thermomechanical instability analysis of inhomogeneous deformation in amorphous alloys. Acta Materialia 55, 2319–2327.

Gu, X., Jian, T., Kecskes, L.J., Woodman, R.H., Fan, C., Ramesh, K.T., Hufnagel, T.C., 2003. Crystallization and mechanical behavior of (Hf, Zr)–Ti–Cu–Ni–Al metallic glasses. Journal of Non-Crystalline Solids 317, 112–117.

He, G., Lu, J., Bian, Z., Chen, D., Chen, G., Tu, G., Chen, G., 2001. Fracture morphology and quenched-in precipitates induced embrittlement in a Zr-based bulk glass. Materials Transactions 42, 356–364.

Helbawi, H., Zhang, L.C., Zarudi, I., 2001. Difference in subsurface damage in indented specimens with and without bonding layer. International Journal of Mechanical Sciences 43, 1107–1121.

Huang, R., Suo, Z., Prevost, J.H., Nix, W.D., 2002. Inhomogeneous deformation in metallic glasses. Journal of the Mechanics and Physics of Solids 50, 1011–1027.

Inoue, A., Zhang, W., Zhang, T., Kurosaka, K., 2001. High-strength Cu-based bulk glassy alloys in Cu-Zr-Ti and Cu-Hf-Ti ternary systems. Acta Materialia 49, 2645–2652.

Jiang, M.Q., Dai, L.H., 2009. On the origin of shear banding instability in metallic glasses. Journal of the Mechanics and Physics of Solids 57, 1267–1292.

Johnson, W.L., Samwer, K., 2005. A universal criterion for plastic yielding of metallic glasses with a $(T/Tg)^{2/3}$ temperature dependence. Physical Review Letters 95, 195501.

Lee, M.L., Li, Y., Schuh, C.A., 2004. Effect of a controlled volume fraction of dendritic phases on tensile and compressive ductility in La-based metallic glass matrix composites. Acta Materialia 52, 4121–4131.

Lewandowski, J.J., Greer, A.L., 2006. Temperature rise at shear bands in metallic glasses. Nature Materials 5, 15–18.

Lewandowski, J.J., Lowhaphandu, P., 2002. Effects of hydrostatic pressure on the flow and fracture of a bulk amorphous metal. Philosophical Magazine A 82, 3427–3441.

Li, H., Subhash, G., Gao, X.-L., Kecskes, L.J., Dowding, R.J., 2003. Negative strain rate sensitivity and compositional dependence of fracture strength in Zr/Hf based bulk metallic glasses. Scripta Materialia 49, 1087–1092.

Liu, L.F., Dai, L.H., bai, Y.L., Wei, B.C., 2005. Initiation and propagation of shear bands in Zr-based bulk metallic glass under quasi-static and dynamic shear loadings. Journal of Non-Crystalline Solids 351, 3259–3270.

Liu, C.T., Heatherly, L., Easton, D.S., Carmichael, C.A., Wright, J.L., Schneibel, J.H., Yoo, M.H., Chen, C.H., Inoue, A., 1998. Test environments and mechanical properties of Zr-base bulk amorphous alloys. Metallurgical and Materials Transactions A 9, 1811–1820.

Liu, Y.H., Wang, G., Wang, R.J., Zhao, D.Q., Pan, M.X., Wang, W.H., 2007. Super plastic bulk metallic glasses at room temperature. Science 315, 1385–1388.

Lu, J., Ravichandran, G., 2003. Pressure-dependent flow behavior of $Zr_{41.2}Ti_{13.8}Cu_{12.5}Ni_{10}Be_{22.5}$ bulk metallic glass. Journal of Material Research 18, 2039–2049.

Lu, J., Ravichandran, G., Johnson, W.L., 2003. Deformation behavior of the $Zr_{41.2}Ti_{13.8}Cu_{12.5}Ni_{10}Be_{22.5}$ bulk metallic glass over a wide range of strain-rates and temperatures. Acta Materialia 51, 3429–3443.

Matsuoka, H., Nakai, T., 1974. Stress-deformation and strength characteristics of soil under three different principal stresses. Proceedings of Japan Society of Civil Engineers 232, 59–70.

Maugin, G.A., 1992. The Thermomechanics of Plasticity and Fracture. Cambridge University Press, Cambridge.

Mukai, T., Nieh, T.G., Kawamura, Y., Inoue, A., Higashi, K., 2002. Effect of strain rate on compressive behavior of a $Pd_{40}Ni_{40}P_{20}$ bulk metallic glass. Intermetallics 10, 1071–1077.

Pan, D., Inoue, A., Sakurai, T., Chen, M.W., 2008. Experimental characterization of shear transformation zones for plastic flow of bulk metallic glasses. Proceedings of the National Academy of Sciences 105, 14769–14772.

Peierls, R.E., 1940. The size of a dislocations. Proceedings of the Physical Society of London 52, 34–37.

Rice, J.R., 1992. Dislocation nucleation from a crack tip – an analysis based on the Peierls concept. Journal of the Mechanics and Physics of Solids 40, 239–271.

Rudnicki, J.W., Rice, J.R., 1975. Conditions for the localization of deformation in pressure-sensitive dilatant materials. Journal of the Mechanics and Physics of Solids 23, 371–394.

Schuh, C.A., Lund, A.C., 2003. Atomistic basis for the plastic yield criterion of metallic glass. Nature Materials 2, 449–452.

Schuh, C.A., Nieh, T.G., 2004. A survey of instrumented indentation studies on metallic glasses. Journal of Materials Research 19, 46–57.

Schuh, C.A., Hufnage, T.C., Ramamurty, U., 2007. Mechanical behavior of amorphous alloys. Acta Materialia, 55.

Shimizu, F., Ogata, S., Li, J., 2006. Yield point of metallic glass. Acta Materialia 54, 4293–4298.

Song, S.X., Bei, H., Wadsworth, J., Nieh, T.G., 2008. Flow serration in a Zr-based bulk metallic glass in compression at low strain rates. Intermetallics 16, 813–818.

Spaepen, F., 1977. A microscopic mechanism for steady state inhomogeneous flow in metallic glasses. Acta Metallurgica, 25.

Steif, P.S., Spaepen, F., Hutchinson, J.W., 1982. Strain localization in amorphous metals. Acta Metallurgica 30, 447–455.

Stillinger, F.H., 1995. A topographic view of supercooled liquids and glass-formation. Science 267, 1935–1939.

Storen, S., Rice, J.R., 1975. Localized necking in thin sheets. Journal of the Mechanics and Physics of Solids 23, 421–441.

Su, C., Anand, L., 2006a. Plane strain indentation of a Zr-based metallic glass: experiments and numerical simulation. Acta Materialia 54, 179–189.

Su, C., Anand, L., 2006b. Plane strain indentation of a Zr-based metallic glass: experiments and numerical simulation. Acta Materialia 54, 179–189.

Sun, B.A., Yu, H.B., Jiao, W., Bai, H.Y., Zhao, D.Q., Wang, W.H., 2010. Plasticity of ductile metallic glasses: a self-organized critical state. Physical Review Letters 105, 035501.

Sunny, G., Lewandowski, J., Prakash, V., 2007. Effects of annealing and specimen geometry on dynamic compression of a Zr-based bulk metallic glass. Journal of Materials Research 22, 389–401.

Sunny, G., Yuan, F., Lewandowski, V.P.J., 2009. Design of inserts for split-Hopkinson pressure bar testing of low strain-to-failure materials. Experimental Mechanics 49, 400–479.

Tandaiya, P., Ramamurty, U., Narasimhan, R., 2009. Mixed mode (I and II) crack tip fields in bulk metallic glasses. Journal of the Mechanics and Physics of Solids 57, 1880–1897.

Thamburaja, P., Ekambaram, R., 2007. Coupled thermo-mechanical modelling of bulk-metallic glasses: theory, finite-element simulations and experimental verification. Journal of the Mechanics and Physics of Solids 55, 1236–1273.

Trexler, M.M., Thadhani, N.N., 2010. Mechanical properties of bulk metallic glasses. Progress in Materials Science 55, 759–839.

Wang, G., Chan, K.C., Xia, L., Yu, P., Shen, J., Wang, W.H., 2009a. Self-organized intermittent plastic flow in bulk metallic glasses. Acta Materialia 57, 6146–6155.

Wang, J.G., Zhao, D.Q., Pan, M.X., Shek, C.H., Wang, W.H., 2009b. Mechanical heterogeneity and mechanism of plasticity in metallic glasses. Applied Physics Letters 94, 031904.

Wright, W.J., Samale, M.W., Hufnagel, T.C., LeBlanc, M.M., Florando, J.N., 2009. Studies of shear band velocity using spatially and temporally resolved measurements of strain during quasistatic compression of a bulk metallic glass. Acta Materialia 57, 4639–4648.

Wu, W.F., Li, Y., Schuh, C.A., 2008. Strength, plasticity and brittleness of bulk metallic glasses under compression, statistical and geometric effects. Philosophical Magazine 88, 71–89.

Yang, Q., Mota, A., Ortiz, M., 2006. A finite-deformation constitutive model of bulk metallic glass plasticity. Computational Mechanics 37, 194–204.

Yao, J.H., Wang, J.Q., Lu, L., Li, Y., 2008. High tensile strength reliability in a bulk metallic glass. Applied Physics Letters 92, 041905.

Ye, J.C., Lu, J., Yang, Y., Liaw, P.K., 2010. Extraction of bulk metallic-glass yield strengths using tapered micropillars in micro-compression experiments. Intermetallics 18, 385–393.

Zhang, Y., Greer, A.L., 2006. Thickness of shear bands in metallic glasses. Applied Physics Letters 89, 071907.

Zhang, Z.F., Eckert, J., Schultz, L., 2003a. Difference in compressive and tensile fracture mechanisms of $Zr_{59}Cu_{20}Al_{10}Ni_8Ti_3$ bulk metallic glass. Acta Materialia, 51.

Zhang, Z.F., He, G., Eckert, J., Schultz, L., 2003b. Fracture mechanisms in bulk metallic glassy materials. Physical Review Letters 91, 045505.

Zhao, M., Li, M., 2008. Interpreting the change in shear band inclination angle in metallic glasses. Applied Physics Letters 93, 241906.

Zink, M., Samwer, K., Johnson, W.L., Mayr, S.G., 2006. Plastic deformation of metallic glasses: size of shear transformation zones from molecular dynamics simulations. Physical Review B 73, 172203.